

# Replay-based Recovery for Autonomous Robotic Vehicles from Sensor Deception Attacks

Pritam Dash\*, Guanpeng Li†, Mehdi Karimibiuki\*, Karthik Pattabiraman\*

\*University of British Columbia

{pdash, mkarimib, karthikp}@ece.ubc.ca

†University of Iowa

guanpeng-li@uiowa.edu

**Abstract**—Sensors are crucial for autonomous operation in robotic vehicles (RV). Physical attacks on sensors such as sensor tampering or spoofing can feed erroneous values to RVs through physical channels, which results in mission failures. In this paper, we present *DeLorean*, a comprehensive diagnosis and recovery framework for securing autonomous RVs from physical attacks. We consider a strong form of physical attack called sensor deception attacks (SDAs), in which the adversary targets multiple sensors of different types simultaneously (even including all sensors). Under SDAs, *DeLorean* inspects the attack induced errors, identifies the targeted sensors, and prevents the erroneous sensor inputs from being used in RV’s feedback control loop. *DeLorean* replays historic state information in the feedback control loop and recovers the RV from attacks. Our evaluation on four real and two simulated RVs shows that *DeLorean* can recover RVs from different attacks, and ensure mission success in 94% of the cases (on average), without any crashes. *DeLorean* incurs low performance, memory and battery overheads.

## I. INTRODUCTION

Autonomous Robotic Vehicles (RV) such as drones and rovers rely on their on-board sensors to perceive their physical states (e.g., position, angular orientation, acceleration). Based on the physical states, specialized algorithms plan the RV’s mission trajectory and autonomously make decisions. Unfortunately, attacks such as sensor tampering and spoofing can feed erroneous sensor measurements through physical channels (henceforth referred to as physical attacks) causing RVs to deviate from their course and/or result in a crash [36], [46]. Physical attacks such as GPS spoofing have been performed against military drones [34] and marine navigation systems [33]. Such attacks cannot be prevented by software security techniques as they target the sensor hardware rather than the software. Physical attacks on sensors can be debilitating for the RV and result in mission failures and crashes [46], which in turn can result in physical damage and injuries.

Prior work has proposed techniques [25], [43] to detect physical attacks on RVs. However, detection alone is not enough, because it does not prevent adverse consequences such as drastic deviation of the RV from its course, and/or crash. Other techniques such as software sensors-based recovery (SSR) [24] and PID-Piper [28] have been proposed for recovering RVs from physical attacks.

Unfortunately, existing recovery techniques suffer from two main weaknesses. First, they are only effective when a single sensor or set of sensors of the same type is under attack, but not when multiple sensors of different types are simultaneously

targeted (as we show later in the paper). The feasibility of attacks targeting multiple sensors simultaneously has been demonstrated on bare metal systems [41] and autonomous driving systems [20]. We extend this attack setting to RVs, and demonstrate the impact of multiple sensor attacks on RVs. We refer to single and multiple sensor attacks as *Sensor Deception Attacks* (SDA). We assume that SDAs can target one or more sensors (including all the sensors) of the RV simultaneously. Second, prior techniques do not perform attack diagnosis to identify which sensors are under attack, and instead, apply their respective recovery strategies blindly. However, it is important to identify the targeted sensors via attack diagnosis and apply the appropriate recovery, particularly under SDAs.

We present *DeLorean*<sup>1</sup>, a framework to diagnose and recover RVs from SDA. *DeLorean* integrates with existing model-based attack detection techniques [25], [28], [43], and provides attack diagnosis and recovery after detection. *DeLorean* is based on the observation that because physical attacks are launched using fake signal emitters (e.g., acoustic, magnetic, or fake GPS), the fake signals are confined to a physical range (i.e., attack zone). Beyond this range, the fake signals are not strong enough to influence the sensors [36], [37], [49]. Furthermore, it is difficult for the attacker to follow the RV and emit fake signals that interfere with the sensors at the resonant frequency [49]. Thus, to recover RVs from attacks, it is sufficient to derive actuator signals to safely maneuver the RV out of the attack zone (i.e., without crashing).

Typically, RVs use specialized algorithms (e.g., state estimation, sensor fusion) to estimate physical states based on sensor measurements, and use a Proportional Integral Derivative (PID) controller to derive the actuator signals (e.g., motor thrust). The PID controller uses the physical states as feedback to minimize environmental noise or error, i.e., a feedback control loop. As attacks manipulate sensor measurements, the corresponding physical states get corrupted. This leads to erroneous actuator signals that result in the RV deviating from its trajectory and/or crashing. There are two main challenges that a recovery technique must address: 1) Preventing erroneous feedback to the PID controller. 2) Deriving safe actuator signals that can maneuver RVs safely out of the attack zone.

*DeLorean* addresses the above challenges through two innovations. First, it uses *factor graphs* [19] to inspect the attack induced errors in the RV’s physical states, identifies the sensors targeted by the attack, and isolates those sensors from

<sup>1</sup>Name inspired by the time machine in the *Back to the future* movies.

the feedback control loop. This prevents erroneous feedback to the PID controller (challenge 1). Factor graphs are graph-based models, which we use for fine-grained representation of conditional dependencies in the RV's past and present states, and to reason about the abnormalities in RV's physical states under attacks. Second, it *replays* a sequence of historic state information collected from an attack-free phase of the RV mission as substitution inputs in the feedback control loop to derive its actuator signals under attacks (challenge 2). This approach is inspired by Dead Reckoning [17], a method for deriving current position and heading direction using past estimates under sensor outages in aircraft systems and ships. Thus, by isolating the sensors under attack and replaying the safe historical states to the PID controller in the feedback loop, the state estimation error remains bounded regardless of the external disturbance. This prevents fluctuations in the actuator signals, and allows the PID controller to derive constant actuator signals and maneuver the RV out of the attack zone.

Note that we consider a strong adversary compared to almost all prior work in this space i.e., the attacker can target all or any combination of the on-board sensors of an RV simultaneously (though within an attack range). *DeLorean* recovers RVs even under this strong adversary model, and ensures both safety and mission success. Our contributions are:

- Propose an attack diagnosis technique that uses factor graphs to examine the past and present states of the RV, and identify the sensors targeted by SDAs.
- Propose an attack recovery technique that replays the sequence of safe historic states in the feedback control loop of the RV.
- Design *DeLorean*, a framework that integrates with existing model-based attack detection techniques and provides both attack diagnosis and recovery.
- Evaluate *DeLorean* on 6 RVs - 4 real systems, and 2 simulated systems on a wide range of scenarios. We compare *DeLorean*'s recovery to prior work on attack recovery in RVs, namely SSR [24] and PID-Piper [28]. Finally, we evaluate the need for and the efficacy of the attack diagnosis performed by *DeLorean*.

Our results are as follows. (1) *DeLorean* recovers RVs from SDAs, and achieves mission success in over 94% of the cases (82% mission success in the worst case attack scenario when all sensors are attacked), while prior work is only effective when 1 or 2 sensors are attacked. Further, *DeLorean* incurs no crashes, unlike prior techniques. (2) *DeLorean* incurs less than 8% CPU overhead and  $\approx 19\%$  battery overhead on average on the 4 real RVs, (3) *DeLorean* successfully recovers RVs from even adaptive attacks (i.e., the attacker knows *DeLorean*'s recovery strategy and deliberately crafts attacks to deceive *DeLorean*), and (4) *DeLorean* achieves much higher recovery rates with attack diagnosis than without. *DeLorean*'s attack diagnosis has 100% true positives, and 10% false positives. In the case of false-positives, the diagnosis triggers gratuitous recovery, and the RV successfully completes the mission.

## II. BACKGROUND AND THREAT MODEL

In this section, we present an RV's state estimation process and the role of various sensors. Then, we present the concept

of a sensor deception attack (SDA), followed by the limitations of existing work, and finally, the threat model.

### A. State Estimation and Control in RVs

Typically, an RVs' state estimation and control process operates in a feedback loop. It uses the sensor measurements to determine the physical state of the vehicle, and derive actuator signals for positioning the vehicle in the next state using mathematical models (Figure 1). For example, GPS measures the RV's position, gyroscope measures angular velocity, accelerometer measures velocity and acceleration, magnetometer measures the heading direction, and barometer measures the altitude based on pressure change. RVs typically use a gyroscope, an accelerometer, and a separate magnetometer for each axis of the vehicle, namely roll (rotation in  $x$  axis), pitch (rotation in  $y$  axis) and yaw (rotation in  $z$  axis).

In addition, RVs use state estimation to enhance the physical state results based on multi-sensor measurements. As mentioned above, a single physical property (e.g., position, angular velocity etc.) is measured by each sensor, and a state estimation or fusion algorithm combines the redundant information to generate a single physical state output with high accuracy. Sensor fusion algorithms (e.g., Extended Kalman Filter [39]) are often used to reduce uncertainty and produce more accurate state estimates.

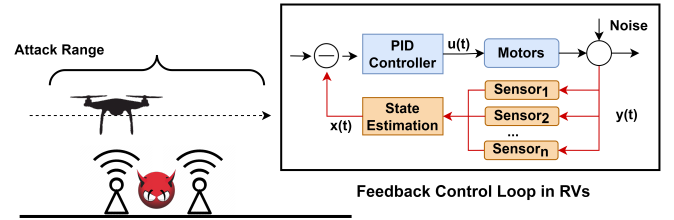


Fig. 1: State Estimation and Feedback Control in RVs. SDA during RV missions.

Because environmental noise may affect an RV's physical state, a PID controller is typically used to minimize the impact of the noise. The PID controller uses the error in the RV's target and physical states, and applies a compensation mechanism to account for the noise when estimating the actuator signals.

### B. Sensor Deception Attack

Physical attacks have been demonstrated against RVs that manipulate sensor measurements from an external source via physical channels (e.g., acoustic or magnetic noise). Physical attacks are often launched by injecting false data (a bias value) to raw sensor measurements [25], [27], [43] as follows.

1. MEMS Gyroscope and MEMS accelerometer sensors that are commonly used in RVs are known to be vulnerable to acoustic noise injection at resonant frequency [46], [48]. These sensors use mechanical structures to detect inertial stimuli and generate electrical signals to depict it. The acoustic noise signal is close to the natural frequency of the mechanical structure forces the sensing mass to resonance. This vulnerability allows an attacker to control the sensor outputs by injecting carefully crafted acoustic signals [49]. A MEMS magnetometer sensor

works with a similar principle and can be manipulated by injecting artificial magnetic field [41].

2. Likewise, GPS spoofing attacks transmit fake and more powerful signals, as a result of which the victim locks onto the fake signal instead of the legitimate GPS signal. Successful spoofing experiments have been carried out in real-world settings [33], [34], often by powerful nation states.

3. False data injection attacks have been theorized against barometer sensors [22]. However, no such attacks have been demonstrated in practice to the best of our knowledge.

In this paper, we consider a strong form of physical attack against RVs which we call *Sensor Deception Attack (SDA)*. In this attack, one or more sensors in the RV are compromised simultaneously, even up to all the sensors. An SDA is launched by injecting malicious signals to the RV's sensors. For example, an adversary can set up a fake GPS emitter, acoustic signal injectors, and magnetic signal injectors at a geographical location, and target the GPS, gyroscope, accelerometer and magnetometer sensors simultaneously during an RV mission. Such an SDA can be debilitating for the RVs, as it *simultaneously* corrupts the physical properties measured by the heterogeneous sensors on the RV (e.g., position, velocity, acceleration, angular velocity, heading direction etc.)

Prior work has demonstrated SDAs targeting multiple sensor types. For example, Nashimoto et al. [41] showed that by targeting gyroscope, accelerometer, and magnetometer sensors at once through acoustic and magnetic signal injection, an adversary can influence the inclination calculation even in the presence of sensor fusion (EKF). We demonstrate later that such an attack can crash a drone almost immediately.

### C. Limitations of Existing Techniques

Existing attack recovery techniques for RVs, PID-Piper [28] and SSR [24], can recover the RV only when a single sensor, or redundant sensors of the same type are attacked simultaneously (shown in Section VI). Thus, they cannot recover from SDAs that target multiple sensors of different types (e.g., GPS and accelerometer).

PID-Piper uses a machine learning (ML) based feed-forward controller (FFC) that prevents attack induced errors in the RV's physical states from affecting actuator signals. Unlike a feedback controller, an FFC does not measure and correct errors. Rather, an FFC anticipates the attack induced error in sensor measurements by correlating past and present states, and derives robust actuator signals proactively to recover RVs.

SSR constructs a system model of the RV that considers controller, actuators and vehicle dynamics. The system model predicts the RV's next state given the current state and target position. The software sensors (i.e., the set of programs that emulate the real sensors such as GPS, gyroscope, accelerometer) take the system model's predictions as input, and derive the measurements similar to the real sensors. Under an attack, the software sensor's outputs are used to recover the RV.

A fundamental issue with both SSR and PID-Piper, is that they use models that approximate the RV's behaviour. Therefore, the model predictions i.e., sensor outputs in the case of SSR and actuator signals in the case of PID-Piper, deviate

slightly from the RV's actual behaviour even in the absence of attacks. This is because there is always an error margin between model estimations and the observed RV behaviour. For PID-Piper, when only one physical property of the RV is manipulated (i.e., single sensor is attacked), the discrepancy in the inputs to the ML model is small enough (i.e., only one or two features are subject to error) that the model can still predict robust actuator signals and recover RVs. However, when multiple sensors are attacked simultaneously, the discrepancy is large and PID-Piper fails to recover from the attack. On the other hand, SSR uses linear models to predict the non-linear RV's behaviour, which has been shown to incur high model inaccuracies [27], [43]. The error in software sensor outputs are small under single sensor attack; however, under multiple sensor attacks, the error builds up and results in erroneous actuator signals. Thus, SSR also fails to recover RVs from SDAs targeting multiple sensors.

Furthermore, neither technique performs any attack diagnosis to determine the faulty sensor. Instead, they apply their respective recovery strategies blindly. This makes it challenging to derive safe actuator signals under multi-sensor SDAs as the recovery technique does not know which sensors are trustworthy. Thus, identifying the targeted sensors, and applying the appropriate corrective measures reduces the error margin compared to blindly applying a corrective measure.

As RVs are often deployed in critical missions, ensuring safety of the vehicle and the stakeholders is paramount. Therefore, recovery techniques must be resilient to even the worst possible attack i.e., all the sensors are compromised simultaneously. *We define a successful mission as one in which the RV reaches the planned destination without crashing despite SDAs (Section V provides more details).*

### D. Threat Model

We focus on physical attacks that maliciously perturb one or more of the RV's sensor measurements to cause deviations or disruptions in its mission. To launch the attacks, attackers can deploy signal emitters in locations of their choosing (Figure 1). However, we assume that the effects of the signal emitters are limited to a range (distance between emitter and RV). This is because malicious GPS signal emitters, acoustic signals etc. are all only effective for a certain range - the malicious signal becomes faint after this range [37], [49]. We further assume that the attacker can increase the attack range using strong emitters [37], [49], or lay out signal emitters at multiple geographical locations. However, we assume that they cannot plant signal emitters all along the RV trajectory.

We assume that the attacker's locations are fixed, and that the attacker cannot follow the RV. This is because it is difficult to move the signals emitters relative to the target RV, and still maintain the resonant frequency of the malicious signals to tamper with the MEMS sensors [49]. Note that all the prior work that demonstrated physical attacks did so with static signal emitters [37], [46], [48], [49]. The attack success drops significantly when signal emitters are in motion [49].

We assume that the attacker has the following capabilities: (1) perform sensor spoofing attacks on GPS or manipulate IMU (gyroscope, accelerometer, magnetometer etc.) sensors of the RV, and (2) can also arbitrarily manipulate one or more

sensor readings to her desired values, and at any time during the RV's mission. However, we exclude attacks that target the software components or firmware, as they can be handled by existing techniques [26]. Further, we assume that the attacker does not have the following capabilities: (1) write access to the firmware, (2) root access to the Operating System (OS).

### III. INITIAL STUDY

In this section, we present an experiment to demonstrate the impact of SDAs on an RV, and how SDAs influence the RV's feedback control loop that results in a crash. Then, we explain our approach to recovering RVs from SDA.

#### A. Experiment

SDA is a strong physical attack that potentially manipulates all the sensor measurements  $y(t)$  thereby corrupting the physical states  $x(t)$  of the RV, and eventually affects the actuator signals  $u(t)$  derived by the PID controller (Figure 1). We perform an experiment to understand how sensor perturbations propagate in the feedback control loop, and corrupt the actuator signals of the RV. In particular, we perform SDA targeting *all* the onboard sensors (i.e., GPS, gyroscope, accelerometer, magnetometer, barometer) of a Sky-viper drone (more details in Section VI). The attack is launched by modifying sensor libraries of the drone's autopilot software [4] as we do not have access to specialized signal emitters (details in Section VI).

In this experiment, the drone was issued the following commands: 1) Take-off, attain an altitude of 10 m, (2) Waypoint, navigate in a straight line towards the target, and (3) Land, when the target is reached. We launch SDA once the drone navigates towards its target in a straight line (i.e., steady state). We intermittently launched 4 instances of SDA at  $t=10s$ ,  $t=20s$ ,  $t=35s$ , and  $t=45s$ , targeting all the onboard sensors. We deliberately perform the attack intermittently to understand the correlation between sensor manipulations, corruption in physical states and corruption of actuator signal. The first 3 instances of SDA lasted for 1s. In contrast, the fourth instance of SDA lasted for more than 5s, which caused the RV to crash.

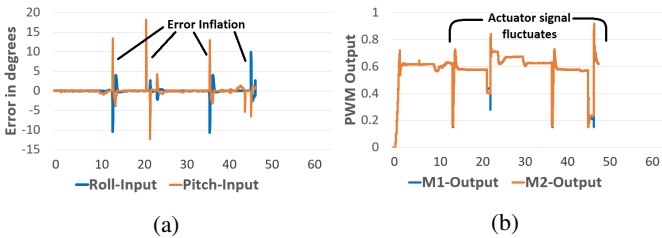


Fig. 2: Impact of SDA, (a) Error inflation in RV's roll and pitch angles, (b) Fluctuations in RV's actuator signal.

Figure 2 shows the impact of SDA on an RV. Recall that the PID controller takes the error between the RV's target and current physical states ( $e_s = target - current$ ) as input, and derives the appropriate actuator signal (Figure 1). Figure 2a shows the  $e_{roll}$  and  $e_{pitch}$ . For simplicity, we show only 2 out of the 18 physical states of the RV. Attack induced sensor manipulations propagate in the RV's feedback control loop and

corrupt the RV's current state estimations. This causes error inflation in  $e_{roll}$  and  $e_{pitch}$  starting  $t=10$  as shown in Figure 2a.

Figure 2b shows the RV's actuator signals. Again, we show only the actuator signals of 2 out of 4 motors in the drone i.e., the Pulse Width Modulation (PWM) values for M1 and M2 in Figure 2b, which are almost identical. In the attack free segment of the mission (0-10s) the  $e_{roll}$  and  $e_{pitch}$  are constant (i.e., 0 as shown in Figure 2a). As the inputs of the PID controller are constant, it derives constant actuator signals e.g., PWM that controls motor speed, which was set at 0.61 (Figure 2b). However, attack induced error inflation in  $e_s$  results in the PID controller deriving erroneous actuator signals. As shown in Figure 2b, the PWM values of M1 and M2 fluctuates between 0.2 and 0.7 which results in a crash. *Thus, attack induced sensor perturbations corrupts the inputs of the PID controller, resulting in unsafe actuator signals.*

#### B. Recovery Requirements

Based on the observations in the above experiment, we derive two requirements for recovering RVs from SDA: **R1** Prevent attack induced sensor manipulations from propagating in the RV's feedback control loop, and **R2** Control the corruption of the PID controller's inputs, and derive safe actuator signals to maneuver the RV out of the attack zone. These two requirements ensure that under attack, the RV can navigate out of the attack zone without crashing.

Our recovery approach contains two steps: First, we isolate the sensors under attack from the feedback control loop via attack diagnosis. This prevents the corrupted sensor measurements from propagating in the RV's feedback control loop (satisfying **R1**). Second, we replay the historic physical states corresponding to the targeted sensors till the RV is out of the attack. The historic states contain information such as the RV's position, velocity, acceleration, angular orientation etc.

Our recovery strategy is inspired by Dead Reckoning [17], a widely used process in aircrafts and ships for calculating the current position and heading direction using previously determined estimates, when sensor information is unavailable. As we have seen, due to erratic error inflation in its inputs under attacks, the PID controller derives erroneous actuator signals. Therefore, by replaying (safe) historic states to the RV's controller, the error  $e_s$  between RV's target state and current physical state remains bounded regardless of the external disturbance unlike in Figure 2a. As a result, the PID controller derives constant actuator signals instead of fluctuating, safely maneuvering the RV out of the attack zone (satisfying **R2**).

For example, in Figure 2, we record the RV's physical states during the attack-free phase of the mission (0-10s). Upon detection, we diagnose the attack to identify the targeted sensors, and replay the safe historic states (0-10s) corresponding to the targeted sensors. In the case of the gyroscope sensor, these physical states would be roll, pitch and yaw angles, roll rate, pitch rate, and yaw rate.

### IV. DESIGN

In this section, we describe the design of the *DeLorean* framework. *DeLorean* is agnostic of the attack detection technique, and can hence be used with any existing model-based



attack detection techniques proposed for RVs e.g., Control Invariants [25], Savior [43], PID-Piper [28]. These techniques have proven to be effective in detecting attacks (i.e, have low false negatives).

*DeLorean* has two main innovations: (i) **Attack Diagnosis**: Under an attack, *DeLorean* identifies the targeted sensors to selectively apply the corrective measures, and (ii) **Historic State Replay**: *DeLorean* replays historic states recorded from an attack-free phase of the mission to control corruption of PID controller's inputs and derive safe actuator signals under attacks. In the attack-free phases of the RV mission, we record the sequence of historic states in a sliding window.

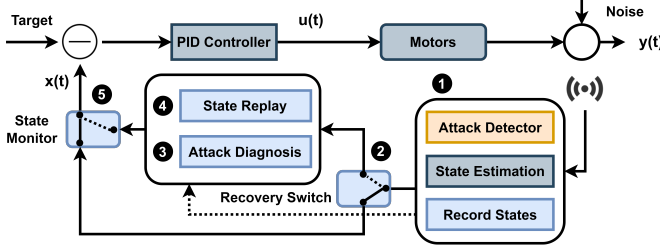


Fig. 3: Feedback control loop with recovery modules

Figure 3 shows the components of *DeLorean*. ① A model-based attack detector uses the sensor measurements  $y(t)$  to derive the RVs next physical state  $x'(t)$ , and compares it with the values derived by the state estimation module  $x(t)$ . If the residual  $r = |x'(t) - x(t)|$  exceeds a predefined threshold, that indicates an attack [25], [28], [43]. Once an attack is detected, ② the *Recovery Switch* activates the ③ *Attack Diagnosis* to identify the sensors under attack, and isolate the targeted sensors from the feedback control loop. This prevents the attack induced sensor manipulations from propagating and causing cascading errors in the feedback control loop.

However, simply removing a stream of inputs from the feedback control loop will disrupt the PID controller's operations and will result in erroneous actuator signals. Therefore, the ④ *State Replay* modules replays a sequence of historic states corresponding to the isolated sensors. ⑤ Finally, the *State Monitor* forwards the physical states  $x(t)$  to the PID controller, after substituting the attacked sensors with their corresponding historical states, until the attack subsides. Replaying the historic states for the attacked sensors controls the error inflation in the inputs of the PID controller. This helps the PID controller maintain constant actuator signals despite the attack, and safely maneuver the RV out of the attack zone.

#### A. Attack Diagnosis

The first step in *DeLorean* is to identify the targeted sensors once an attack is detected. Attack induced sensor manipulations corrupt the RV's physical states that are estimated using the targeted sensors. For example, when the gyroscope sensor is under attack, it leads to the corruption of the RV's Euler angles (roll, pitch, yaw), and angular velocity. We observe that in attack-free segments of the mission, the error between the RV's past and present physical states is largely constant i.e,  $e = |\text{past states} - \text{present states}| = c \pm \epsilon$ , where  $\epsilon$  is environmental noise. However, under attack, the error  $e$  increases i.e,  $e \gg$

$c$  [25], [28], [43]. Our approach for attack diagnosis is to monitor the inflation in error  $e$  for all the physical states of the RV  $(x, y, z, \dot{x}, \dot{y}, \dot{z}, \ddot{x}, \ddot{y}, \ddot{z}, \phi, \theta, \psi, \omega_\phi, \omega_\theta, \omega_\psi, x_m, y_m, z_m)$ . If we observe inflation in error  $e$  for certain physical states, we conclude that the corresponding sensor is under attack. For example, if  $e_{\text{roll}}$  and/or  $e_{\text{pitch}}$  is high, we can conclude that the gyroscope sensor is under attack.

However, error inflation in the RV's physical states can also occur due to environmental noise and faults (overshooting), and not only attacks. Thus, it is important to capture the causal relationship between the observed error  $e$  in RV's physical states and the probable outcome  $s$  (i.e, whether the corresponding sensor is under attack given the observed error  $e$ ). We consider binary outcomes for the sensors i.e, *malicious* (under attack) or *benign* (attack-free). We use factor graphs (FG) to model the causal relationship between  $e$  and  $s$ , and to reason about the error inflation in the RV's physical states. FGs are probabilistic graphical models that allow expressing conditional relationships between variables [19].

The causal relationship between  $e$  and  $s$  can be expressed as a conditional probability problem i.e,  $P(s|e)$ . There are two ways to calculate conditional probability: (1) Using Joint Probability distribution over the observed sequence of  $e$ , and the probable outcomes  $s$  (i.e, benign or malicious sensors). However, expressing the joint probability distribution at run-time for a binary outcome will require  $2^n$  functions i.e, as the mission progresses ( $t = 0$  to  $t = n$ ), the number of functions will increase exponentially, which will have high computation and storage overheads. Therefore, this approach will not work. (2) Using Bayesian approach we can calculate  $P(s|e)$  based on the values of known probabilities of  $P(e|s = \text{malicious})$  and  $P(e|s = \text{benign})$ . We will need to run a large number of experiments and profile the observed error  $e$  in RV's physical states under attacks as well as in absence of attacks to calculate  $P(e|s = \text{malicious})$  and  $P(e|s = \text{benign})$ . This will also not work in our case due to two reasons: First, it is difficult to know how many observations are enough. Second, if we observe an error during inference that was not observed in profiling, the Bayesian approach will assign it a zero probability (i.e, Zero Frequency). This means even if a sensor is under attack, the Bayesian approach will conclude the sensor is benign.

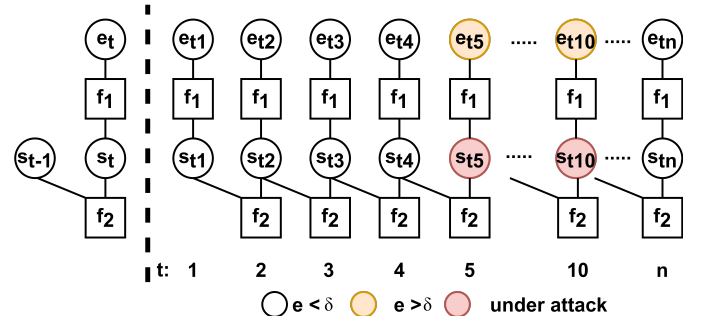


Fig. 4: The graph on the left shows the factor graph for attack diagnosis. The graph on the right shows the factor graph as the mission progresses.

In contrast, FGs allow fine-grained representation of the complex joint probability distribution between variables through a product of smaller probability distributions. Thus,

they incur low computation and storage overheads. Unlike Bayesian approaches that rely on profiling, FGs use functions (known as factor functions) to express conditional relationships. Thus, FGs do not suffer from the Zero Frequency problem. This is why we use FGs for attack diagnosis.

Figure 4 shows an example of FG-based diagnosis for one sensor. The FG represents the relationships between a sequential error  $E = (e_{t_1}, \dots, e_{t_n})$  and the probable outcome  $S = (s_{t_1}, \dots, s_{t_n})$  using bipartite graph. Factor functions  $F = (f_1, f_2)$  define relationships between sequence of error and probable outcomes. Given the observed error, the probable outcome for the sensor is estimated by selecting a configuration of the FG that maximizes the joint probability distribution  $P(E, S)$ . We use Maximum Likelihood Estimation for inference on the FG, and deduce which sensors are under attack.

**Factor Graph Construction** The steps involved in constructing the FGs and using FGs for attack diagnosis are as follows.

*Step 1 - Express the causal relationships between errors in RV's physical states and the probable outcome using factor functions.* To express such a relationship, the first step is to determine the safe and unsafe ranges of the error  $e$ . We collect attack-free RV mission traces, and observe the variation in error  $e$ . Recall that in an attack free phase, the error is mostly constant  $e = c + \epsilon$ , where  $\epsilon$  is environmental noise. We deem  $e$  to be in the safe range if  $0 < e < \delta$ , where  $\delta = \text{median}(e) + k * \text{stdev}(e)$ . The value of  $\delta$  is RV specific and it is derived empirically (details in Section VI). The factor functions rely on the  $\delta$  values of the respective sensors to determine whether the sensors are under attack. Each factor function takes as inputs the observed error and *all* possible outcomes, and outputs a discrete value indicating the relations among the inputs (Equations 1 and 2). In particular, the factor function expresses two relations, (1) if  $e_t > \delta$ , then what is the most probable outcome for the sensor (malicious or benign)? (2) If the sensor was under attack at  $t - 1$ , what is the most probable outcome for the sensor at time  $t$ ?

$$f_1(e_t, s_t) = \begin{cases} 1, & e_t > \delta \text{ and if } s_t = \text{malicious} \\ 0, & \text{otherwise} \end{cases} \quad (1)$$

$$f_2(e_t, s_t) = \begin{cases} 1, & s_{t-1} = \text{malicious and } s_t = \text{malicious} \\ 0, & \text{otherwise} \end{cases} \quad (2)$$

*Step 2 - Construct per sensor factor graphs.* We repeat Step-1 and construct FGs expressing relationships between the error  $e$  and the probable outcome for all the physical states i.e.,  $[x, y, z, \dot{x}, \dot{y}, \dot{z}, \ddot{x}, \ddot{y}, \ddot{z}, \phi, \theta, \psi, \omega_\phi, \omega_\theta, \omega_\psi, x_m, y_m, z_m]$  corresponding to all the sensors of the RV. The factor function shown in Equation 1 and Equation 2 are used for this purpose (only the value of  $\delta$  changes, which is empirically determined).

*Step 3 - Perform inference on the factor graphs to diagnose the targeted sensors.* We feed the physical states derived from sensor measurements to the per sensor FGs to determine the targeted sensors. The joint probability distribution  $P(E, S)$  can be factorized as shown in Equation 3, where  $a$  is input to the factor functions  $\in F$ . The inputs are (1) observed error  $e$ , and (2) the probable outcome  $s$ .

$$P(E, S) = \prod_{f \in F} f(a) \quad (3)$$

At each time  $t$ , the conditional probability can be expressed as  $P(s_t|e_t) = f_1(e_t, s_t) \cdot f_2(s_{t-1}, s_t)$ . We use Maximum Likelihood Estimation (MLE) to find the optimal configuration of the FG, thus identifying the targeted sensor. The most probable outcome for  $s_t$  is found by enumerating all possible sequences of the outcome variables (i.e, benign and malicious), and finding the one that maximizes  $P(s_t|e_t)$  as shown below.

$$s_t = \underset{f \in F}{\operatorname{argmax}}_{s_t} \prod f(a) \quad (4)$$

Probable $s_{t-1}$	Probable $s_t$	$f_1$	$f_2$
benign	benign	0	0
benign	malicious	1	0
malicious	benign	0	0
malicious	malicious	1	1

TABLE I: Enumerating all possible sequence of  $s_{t-1}$  and  $s_t$

At each time step, we input the observed error  $e_t$ , and enumerate all possible outcomes of the  $s_t$  and  $s_{t-1}$ . Consider the example shown in Figure 4. At each time step, the function  $f_1$  takes two inputs,  $a_1$  and  $a_2$ . Where  $a_1 : e_t = \text{observed error}$ ,  $s_1 = \text{benign}$ , and  $a_2 : e_t = \text{observed error}$ ,  $s_1 = \text{malicious}$ . The function  $f_2$  takes 4 inputs,  $a_1, a_2, a_3$ , and  $a_4$ . Where  $a_1 : s_{t-1} = \text{benign}$ ,  $s_t = \text{benign}$ ,  $a_2 : s_{t-1} = \text{benign}$ ,  $s_t = \text{malicious}$ ,  $a_3 : s_{t-1} = \text{malicious}$ ,  $s_t = \text{benign}$ , and  $a_4 : s_{t-1} = \text{malicious}$ ,  $s_t = \text{malicious}$ . At  $t_5$ , the observed error  $e_{t_5}$  becomes greater than  $\delta$ . Table I shows all possible sequence of  $s_{t-1}$  and  $s_t$ . At  $t_5$ , the configuration of FG that maximizes the  $P(s_t|e_t)$  is  $s_t = \text{malicious}$ . Similarly, the configuration of FG that maximizes the  $P(s_{t-1}, s_t|e_{t-1}, e_t)$  is  $s_t = \text{malicious}$ ,  $s_{t-1} = \text{malicious}$ . This indicates that the sensor is under attack.

The above inference is performed on all the per sensor FGs, and if ( $s_t = \text{malicious}$ ) maximizes the  $P(s_t|e_t)$ , then those sensors are deemed to be under attack. This identifies the set of attacked sensors. More details about factor graphs are presented in Appendix IX-A.

## B. Historic State Replay for Recovery

When the RV is in an attack free phase, we record the sequence of physical states estimated from all the on-board sensors in a sliding window. Figure 5a shows the details. The physical states at time  $t$  are represented as  $x(t)$ , and the historic physical states recorded in a window are represented as  $HS$ . The historic states  $HS$  consist of the RV's position  $(x, y, z)$ , velocity  $(\dot{x}, \dot{y}, \dot{z})$ , acceleration  $(\ddot{x}, \ddot{y}, \ddot{z})$ , Euler angles  $(\phi, \theta, \psi)$ , angular velocities (rotation speed of the motors  $\omega_\phi, \omega_\theta, \omega_\psi$ ), and magnetic fields  $x_m, y_m, z_m$ . We record the RV's relative position (distance traveled) not the absolute GPS coordinates.  $HS = [x, y, z, \dot{x}, \dot{y}, \dot{z}, \ddot{x}, \ddot{y}, \ddot{z}, \phi, \theta, \psi, \omega_\phi, \omega_\theta, \omega_\psi, x_m, y_m, z_m]$

When the RV's mission starts, if no alert is raised by the attack detector, starting at  $t_w$  we record  $x(t)$ . We save the  $HS$  recorded in window  $w_i$  and proceed recording states in the next window  $w_{i+1}$ . At the end of window  $w_{i+1}$ , we discard the  $HS$  recorded in the previous window  $w_i$ . Upon detecting an attack we stop recording, and we discard the states recorded in the current window  $w_i$  as they are corrupted by the attack (Figure 5b). We replay the  $HS$  recorded in the previous

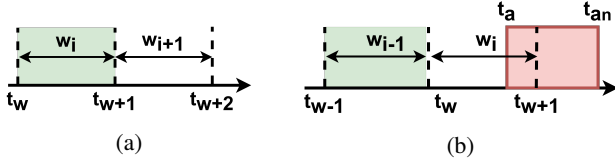


Fig. 5: Recording historic physical states in a sliding window.

window  $w_{i-1}$  for recovery which is attack-free (as no alert was raised by the attack detector), and is hence uncorrupted.

However, it is possible for an attack to span over multiple sliding windows, in which case, it will be challenging to ensure attack-free  $HS$  for recovery. Such stealthy attacks [27] can inject seemingly benign and controlled bias in the sensor measurements over a long time, thereby evading detection, and causing disruption in the RV's mission. Attack detection techniques such as Savior [43] and PID-Piper [28] can detect stealthy attacks using cumulative sum statistics (CUSUM). However, there is necessarily a delay in attack detection i.e., the time interval between the onset of the stealthy attack and the time when the attack detector raises an alert. Due to the detection delay, *DeLorean* might record corrupted  $HS$  for recovery, which it incorrectly deemed safe as no alarms were raised by the attack detector. Therefore, to handle stealthy attacks, we set the window length to be large enough that stealthy attacks can be detected in a single sliding window (details in Section V-B).

Another challenge is that sensors in RVs are sampled at different rates e.g., for critical sensors such as gyroscopes, the sampling rate is 400 Hz, whereas, for non-critical sensors such as barometers, the sampling rate is 100 Hz. It is important to align the data streams when recording the historic states; otherwise, the historic state replay will not result in bounded error between the current and targeted physical states of the RV. To address this problem, we select a single target frequency for recording the  $HS$ , which is the highest sampling rate of all the sensors. We then align the low frequency data streams with the high frequency data streams by inserting data points in the low frequency data stream to match the sample points in the high frequency data streams. In particular, we duplicate the last data point in the low frequency data streams based on the range of the sample points of the high frequency data streams. This aligns the  $HS$  used for recovery.

### C. Algorithm

Algorithm 1 shows *DeLorean*'s algorithm for attack diagnosis and recovery. In the absence of attacks (based on the attack detector's response), *DeLorean* records the physical states associated with all the on-board sensors (Line 7-15) in a sliding window. Once the attack detector raises an alert, *DeLorean* activates recovery mode (Line 17). First, it stops recording, and prepares the most recent safe  $HS$  for recovery. Then, it activates the diagnosis procedure (Line 20). The attack diagnosis module determines the sensors under attack using FGs (Line 27-33). Once the targeted sensors are determined, *DeLorean* identifies the corresponding physical states, and replays the historic states only for those sensors as feedback

### Algorithm 1 Algorithm for Attack Diagnosis and Recovery

```

1:  $w \leftarrow$  historic state recording window
2:  $S \leftarrow$  historic physical states used for recovery
3:  $Tx \leftarrow$  physical states corresponding to targeted sensors
4: procedure HISTORICSTATEPLAY
5:    $alert \leftarrow AttackDetector()$ 
6:   while  $\neg mission\_end$  do
7:     if  $\neg alert$  then ▷ recording historic states
8:        $recovery\_mode \leftarrow false$ 
9:       if  $t_w < t_{w+1}$  then
10:         $record \leftarrow true$ 
11:         $w_i[.] \leftarrow x(t)$ 
12:       else
13:         $delete\ w_{i-1}$ 
14:         $t_w = t_{w+1}$ 
15:       end if
16:     else
17:        $recovery\_mode \leftarrow true$  ▷ recovery activated
18:        $record \leftarrow False$ 
19:        $HS = w_{i-1}$ 
20:        $targetedSensors \leftarrow Diagnosis()$ 
21:        $Tx \leftarrow targetedSensors$ 
22:        $Tx[.] \leftarrow HS[.]$  ▷ replaying for targeted sensors
23:     end if
24:   end while
25: end procedure
26: procedure DIAGNOSIS
27:   while  $\neg mission\_end \ \forall \ sensors \ do$ 
28:      $e = |(e_t) - (e_{t-1})|$ 
29:      $s_t \leftarrow argmax P(s_t|e)$  ▷ most probable outcome
30:     if  $s_t = 1$  then
31:       return malicious ▷ targeted sensors
32:     end if
33:   end while
34: end procedure

```

to the PID controller. Once the attack subsides (based on the attack detector's response), the recovery mode is turned off.

### D. Course Correction

Because *DeLorean* replays historic states to derive constant (non fluctuating) actuator signals for safely maneuvering the RV under SDA, it may cause the RV to veer off its planned trajectory. For example, in Figure 6a, the RV was supposed to turn left in the attack zone. However, because of the attack and subsequent recovery, the RV will miss the turn and continue straight. To address this issue, we add a course correction component that recalculates the RV's trajectory to reach its destination after it leaves the attack zone.

The course correction algorithm uses the Dijkstra's shortest path algorithm to find the shortest path to the destination from the new coordinates of the RV after it has left the attack zone. However, it is possible that the shortest path to the destination takes the RV back to the attack zone, which is not desirable. We prevent the RV from going back to the attack zone by increasing the weights of the paths through the attack zone, which makes them much more expensive. Hence, they will be avoided by the shortest path algorithm (as shown in Figure 6b, value of  $W$  is determined based on  $D$ ). Algorithm for course correction is presented in Appendix IX-C.

Figure 6 shows the course correction procedure. The main steps are as follows: i) At the start of the mission, we calculate the distance  $D$  to the destination as per the defined trajectory. ii) We keep track of the distance traveled  $d_t$  as the mission progresses, and the distance left to cover as  $d_g$  ( $d_g = D - d_t$ ).

iii) When recovery is activated, we stop updating  $d_t$ , and we keep track of the distance traveled under the attack  $d_a$ . iv) When the RV is out of the attack zone (based on the attack detector's response), we recalculate  $d_g$  and check if  $D > d_t + d_a + d_g$ . If the condition is true, it means the RV has veered from its trajectory, and hence we recalculate the path.

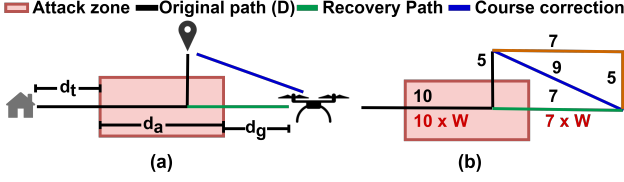


Fig. 6: (a) Course correction after the RV is out of the attack zone. (b) Shows the available paths, and how *DeLorean* finds the shortest path for course correction.

There is one corner case in the course correction procedure where the RV might miss its destination. If the RV's destination is itself in the attack zone, due to recovery activation, the RV will keep moving forward instead of completing the mission. To handle this scenario, we check if the total distance traveled without recovery and with recovery is  $\geq D$  ( $d_t + d_a \geq D$ ). If the above condition is true, we signal to the autopilot that the RV has reached its target, and the mission is completed.

## V. EXPERIMENTAL SETUP AND ATTACK PARAMETERS

### A. Experimental Setup

To evaluate *DeLorean*, we use six RV systems, four of which are real RVs. These are shown in Figure 7, and are (from the left in the figure), (1) Pixhawk based DIY drone [40] (Pixhawk drone), (2) Tarot 650 drone [11] (Tarot drone) (3) Aion R1 ground rover [2] (Aion rover), and (4) Sky Viper Journey drone [9] (Sky-viper drone). These are all commodity RV systems, each costing between \$200 and \$2500. The first three RVs are based on the Pixhawk platform [40]. The Sky-viper drone is based on an STM32 processor. These are equipped with the following five sensors: GPS, gyroscope, accelerometer, barometer and magnetometer. Each RV has different number of sensors, and there is some redundancy among the sensors. Table II shows the details.



Fig. 7: Real RV Systems used for our experiments

The other two systems are simulated RVs, (4) Ardupilot's quadcopter (ArduCopter), and (5) Ardupilot's ground rover [4] (ArduRover). We use the APM SITL [4], and Gazebo [5] platforms for vehicle simulations, and we run them on a Intel Core i7 CPU @ 2.60GHz machine with 32 GB RAM.

**RV Missions** We run a diverse set of missions for each RV with varying mission durations, mission distances, and environmental conditions (e.g., noisy sensor data). Our evaluation covers a variety of mission paths e.g., straight line, circular paths, flights in polygonal paths, and flights with

multiple destinations (or waypoints). These emulate various kinds of real-world RV missions: (1) a last mile delivery drone [35] (straight line path, polygonal path), (2) drones used for surveillance or agriculture [1] (circular or polygonal path), and (3) rovers deployed in warehouse management [3] (polygonal paths). Each mission path is more or less equally represented in the set (Appendix IX-D).

**Comparison** We quantitatively compare our results with both SSR [24], and PID-Piper [28], which are recovery techniques for RVs. Because SSR is not publicly available, we implemented it using Matlab's system identification (SI) tool [10] with our best effort. We collected RV mission traces (training and testing sets) and derived the system model (containing sets of matrices) using the training set. We validated the system model's accuracy with the testing set. For PID-Piper, we used the publicly available implementation [8]. For a fair comparison, we adopted the original autopilot and simulation platforms that were used by SSR and PID-Piper. Because both SSR and PID-Piper incur crashes due to SDAs (Section VI-B), we do not run them in real RVs to prevent damage to the RVs.

**Success Metric** As done by prior work [28], we consider a mission to be successful, if upon completion, the total deviation from the original destination is *less than 10m*. Most GPS sensors used in commodity RVs have an offset of 5 meters [7]. We consider 2X of the GPS offset as our threshold i.e., 5m offset from the RV's position, and 5m offset from the destination. This threshold is indistinguishable from the standard GPS error [7]. We consider the mission to be unsuccessful if the RV crashes (potential physically damaged) or stalls (freezes and stops advancing towards the destination).

**Runtime Overheads:** We measure the overheads in CPU, battery consumption, and memory incurred by the RV due to *DeLorean*. As the overheads in simulated RVs depend on the computing platform, we report the overheads for real RVs. For CPU overheads, we measure the CPU times incurred by the autopilot modules with and without *DeLorean*. During recovery, due to the historic state replay, the motor rotation rates increase compared to the attack-free phase. We call this the operational overhead. We estimate the battery overhead based on both the CPU overhead and the operational overhead. Finally, we estimate the additional memory required to store the historic states for replay.

### B. Attack Parameters

**Attacks** As we did not have access to special equipment (e.g., noise emitter, sound source, amplifier, etc.) for mounting physical attacks, we emulated the attacks through targeted software modifications, similar to what most prior work has done [24], [25], [28], [43]. Our attack code interfaces with the sensor libraries in the RV, and manipulates sensor measurements by adding a bias (i.e., false data). When an attack command is initiated, the bias values are automatically added to the raw sensor measurements. We derive the attack parameters i.e., bias value, attack range and attack duration to mimic physical attacks via software as closely as possible as follows.

**Sensor Bias Values** We use the maximum bias values for each sensor within the allowable range as per the respective sensor specifications. Table II shows the details. For example, the update frequency of the GPS module used in many industrial



TABLE II: Subject RVs in Evaluation, Attack parameters. P: Pixhawk drone, T: Tarot drone, S: Sky-viper drone, AC: ArduCopter, R1: R1 rover, AR: ArduRover

Sensor Type	Number of Sensors						Max Bias Values	Max Range
	P	T	S	AC	R1	AR		
GPS	1	1	1	1	1	1	50m	200
Gyroscope	3	3	1	3	3	3	9.47 rad	100
Accelerometer	3	3	1	3	3	3	6.2 rad/s <sup>2</sup>	26
Magnetometer	3	3	1	1	3	1	180 deg	-
Barometer	1	2	1	1	1	1	0.1 kPa	-

and commodity RVs is 0.1s, and the operational limit in its velocity is 500 m/s [12]. Therefore, the maximum hopping distance of the GPS receiver is 50m (update frequency  $\times$  maximum velocity). Thus, for GPS we set the bias value to be just below 50m, which is the operating limit of the GPS. Table II shows the maximum bias value used for each sensor.

**Attack Range** We derive the maximum attack range based on prior work that performed the respective attacks through signal injection [41], [42], [47]. We extrapolate their results considering the largest available signal source and amplifier to derive the maximum attack range for each sensor. We found that the optimal attack range for individual sensors is within 26 – 200m. Of all the sensors, the GPS has the maximum attack range [47] of 200m. *Thus, we select 200m as the attack range in our experiments i.e, we assume that attackers can manipulate all the sensors in a 200m range.* This is a stronger assumption than that reported in prior work [46], [49]. For example, Son et al. [49] reported the attack range for gyroscope to be around 30m. We extrapolate their results and find that if the attacker uses the largest available sound source that produces 140dB output, the attack range will be at most 100m ( $>150$  dB sound output will rupture the eardrum) [6]. Similarly, attack range of accelerometer can be extended to 24m by using the largest sound source [49]. No prior work has reported an attack range for magnetometer and barometer.

**Attack Duration** We calculate the attack duration based on the time taken by each subject RV to cover the attack range distance. Most of our RVs travel at a velocity of 10m/s speed, and thus, they take about 20s to cover 200m. *Therefore, we set the maximum duration of an individual SDA to 20s.*

## VI. RESULTS

In this section, we first present implementation of *DeLorean* modules, and experimentally derive their parameters. We compare the recovery performed by *DeLorean* with other techniques on simulated RVs. Then, we present *DeLorean*'s recovery on real RVs, and its overheads. We also study the need and effectiveness of attack diagnosis performed by *DeLorean*. Finally, we present *DeLorean*'s efficacy under adaptive attacks.

### A. DeLorean Modules

As mentioned, *DeLorean* is agnostic of the attack detection technique, and provides attack diagnosis and attack recovery after an attack detector raises an alarm. We choose PID-Piper's attack detection module, and integrate it with our framework (Figure 3), as it represents the state-of-the-art. We developed the attack diagnosis module in Python, and the

attack recovery module in C++. We plugged both of these into the RV's feedback control loop, and experimentally derive their parameters as follows.

**Attack Diagnosis** For attack diagnosis, we monitor the error  $e$  between the past and present states of the RV. Recall that in the attack-free phase,  $e$  remains within  $0 - \delta$ . We use the standard deviation method to derive the value of  $\delta$  as  $\delta = \text{median}(e) + k * \text{stdev}(e)$  i.e, if the error  $e$  is more than  $k$  times the standard deviation away from the mean, it is likely to be an outlier (due to the attack) [44]. We collect attack-free RV mission traces (on both simulated and real RVs with diverse mission trajectories), and empirically determine that  $k = 3$  ensures  $0 < e < \delta$  in the attack-free phase of the mission.

Figure 8 shows an example of  $\delta$  for position error and pitch angle in the Pixhawk drone. The figure shows the Cumulative Distribution Function (CDF) of error  $e$  as a function of the probability that the physical states errors will take a value less than  $\delta$ . With  $k = 3$ , we obtain the  $\delta$  values for  $z$ -axis position error as 5.2 and 9.81 for pitch angle error. As shown in Figure 8, in the attack-free phase, the error  $e$  always remains under the  $\delta$  value. We derive  $\delta$  for all the physical states of the RV in the same manner as presented in Appendix IX-D.

To calculate the above values, for each simulated RV, we run 60 missions, each of which lasts for 120s (on average). For the real RV, we run between 15-25 missions across RVs, lasting 50-90s each. Therefore, the total effort for calculating  $\delta$  is about 120 minutes for each simulated RV, and about 28 minutes for each real RV. This is a one time cost for each RV.

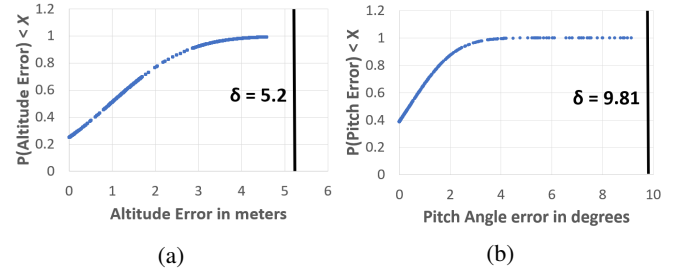


Fig. 8: CDF of error distribution in the Pixhawk drone.  $k = 3$  ensures  $0 < e < \delta$  in attack-free phase.

**Attack Recovery** Recall that the window size must be large enough that a stealthy attack can be detected in a single sliding window (Section IV-B). Therefore, to find the appropriate window size, we launched stealthy attacks on PID-Piper's attack detector. Our goal is to identify the stealthy attack duration, where the attacker corrupts sensor measurements and causes disruptions in the RV mission. Note that PID-Piper uses CUSUM to detect stealthy attacks [27], which is described as:  $S_{t+1} = S_t + |y_{pred}(t) - y_{act}(t)| - b(t)$  where  $S(0) = 0$ , if  $S(t) > \tau$  an alarm is raised, and  $b(t) > 0$  is a parameter that prevents  $S(t)$  from triggering the threshold ( $\tau$ ) due to environmental noise. Thus, the stealthy attacks can be described as  $y^a(t) = y(t) \pm (\tau + b - S(t))$ , where the attacker modifies  $y(t)$  and maintains  $S(t) < \tau$  [43].

First, we performed experiments in all the subject RVs, and launched stealthy attacks targeting all the sensors simultaneously. We find that when all the sensors are manipulated

persistently, the stealthy attack is detected in under 3.3s. We then injected sensor manipulations intermittently and observed how long the stealthy attack can evade detection while causing disruptions. We found that even when launched intermittently, the stealthy attack is detected in under 10s.

Therefore, we performed stealthy attacks in all the subject RVs targeting each sensor individually. We found that (1) Stealthy attacks targeting barometer and magnetometer sensors did not cause any observable disruption in the RV's trajectory. (2) Stealthy attacks against gyroscope and accelerometer sensors caused the RV to shake vigorously and veer off from its trajectory. However, the attacks were detected in under 13s and did not cause any crash. (3) Stealthy attacks against GPS remain undetected for the maximum duration i.e., around 15–18s. *Therefore, we select the window size to be larger than the time taken to detect stealthy attacks against GPS.* Table III shows the window size  $w$  derived for each subject RV.

TABLE III: Recording window size for each subject RV. P: Pixhawk drone, T: Tarot drone, S: Sky-viper drone, AC: ArduCopter, R1: R1 rover, AR: ArduRover. WS: Window size

	P	T	S	R1	AC	AR
WS	15.5s	15s	17s	18.5s	15.5s	17s

Historic states replay controls the errors in PID controller's inputs that in turn derives safe actuator signals. Due to space constraints more details are presented in Appendix IX-E. In situations where the recorded states are insufficient to maneuver the RV i.e., the attack duration  $> w$ , we iteratively replay the historic states till the RV is out of the attack zone.

#### B. Comparison of DeLorean, SSR and PID-Piper under SDAs

To understand the impact of SDAs on the RVs, we perform experiments on the two simulated RVs, without any protection. First, we performed SDAs targeting each individual sensor by injecting the maximum bias values in Table II. We find that even SDAs targeting a single sensor resulted in mission failures (in all cases). We then perform SDAs targeting different combination of sensors up to and including all the sensors. Unsurprisingly, these also resulted in mission failures.

We then compare *DeLorean* with SSR and PID-Piper in recovering from the SDAs on the simulated RVs. We did not use real RVs in this experiment as we encountered crashes in the simulations for SSR and PID-Piper, hence did not want to damage the real RVs. We launched 75 missions for simulated RVs protected with SSR, PID-Piper and *DeLorean* respectively. We mounted the same attacks for all three techniques varying the number of sensor types targeted from 1 to 5 (all sensors). Note that when we say a sensor is attacked, we mean all the redundant sensors of that type in the RV is attacked.

Table IV shows the mission outcomes of *DeLorean*, SSR and PID-Piper. From the table, SSR has a 64% mission success rate for single sensor attacks. However, for attacks targeting two sensors, its mission success rate drops to 20% with a crash rate of 56%. PID-Piper is 100% effective when only a single sensor is targeted. However, its mission success rate also drops to 20% and its crash rate increases to 64% when two sensors are attacked. Furthermore, when more than two

TABLE IV: *DeLorean*'s recovery outcomes compared with SSR and PID-Piper, as a function of the number of sensors attacked. MS: Mission Success, values are percentages.

# of sensors targeted	SSR		PID-Piper		DeLorean	
	Crash	MS	Crash	MS	Crash	MS
1	20	64	0	100	0	100
2	56	20	64	20	0	100
3	100	0	100	0	0	100
4	100	0	100	0	0	88
5	100	0	100	0	0	82

sensors are targeted, both SSR and PID-Piper incurred a 100% crash rate. Thus, *SSR and PID-Piper incur both crashes and mission failures* for SDAs targeting 2 or more sensors.

In contrast, *DeLorean* incurs *no crashes* in any of the attacks even when all sensors are targeted. Further, *DeLorean* achieves 94% mission success rate on average across all sensor numbers, which is  $\approx 4X$  higher mission success rate than both SSR and PID-Piper. In fact, *DeLorean* achieves 100% mission success when three or fewer sensors are targeted. When four sensors are targeted, *DeLorean* achieves 88% mission success. Even when all sensors are targeted, *DeLorean* achieves 82% mission success.

#### C. DeLorean Recovery in Real RVs

We also evaluate *DeLorean* on the real RVs in various scenarios. We know from the simulation results that RVs protected with *DeLorean* incurred no crashes during simulation, so we do not have to worry about damaging the RVs (this was also confirmed by our experiments). Table V shows *DeLorean*'s recovery outcomes on the four real RV systems. Due to space constraints, we only consider two cases: (1) single sensor SDAs, and (2) multi-sensor SDAs that target all the sensors (i.e., the worst case). We find that for both single sensor and multi-sensor SDAs, *DeLorean* incurred *no crashes*. Further, *DeLorean* achieves 100% mission success for single sensor SDAs, and a mission success rate between 80 and 90% (average of 86.25%) for SDAs targeting all sensors. These results are comparable to the results of *DeLorean* on the simulated RVs. Furthermore, even for the failed missions, the deviation from the target was very small (15.6m on average).

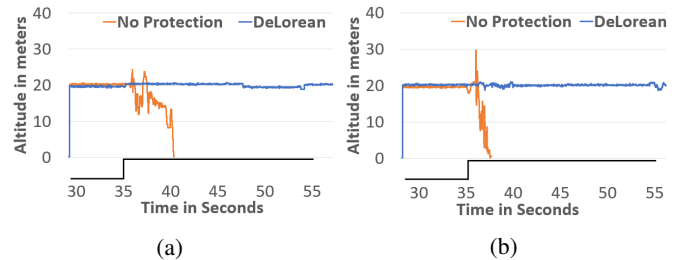


Fig. 9: *DeLorean*'s recovery in the Sky-viper drone: (a) under SDA targeting only GPS sensor, and (b) an SDA targeting all the sensors. Both attacks launched at 35s (bottom graph).

We discuss a couple of cases to understand *DeLorean* recovery on real RVs. Figures 9a and 9b show *DeLorean*

recovery for the Sky-viper drone for a single-sensor SDA and an SDA targeting all sensors. The bottom portion of the graph shows when the attack starts (after 35s). In both the cases, the drone attains 20m elevation after take-off, and navigates towards the target. As can be seen, in both the cases, without *DeLorean*, the drone crashes (altitude drops from 20 to 0m). However, with *DeLorean*, the drone recovers from both types of attacks without crashing (altitude is maintained at 20m).

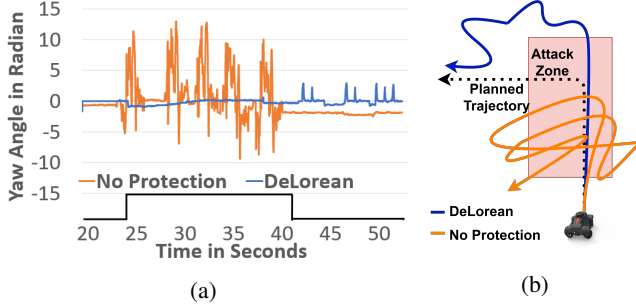


Fig. 10: *DeLorean*'s recovery in Aion rover under SDAs. (a) Yaw angles with and without *DeLorean*, SDA launched 25-40s (bottom graph). (b) Rover's trajectory under recovery.

Figure 10 shows *DeLorean*'s recovery on the Aion rover. In this mission, the rover should head straight and make a left turn. Figure 10b shows the mission trajectory under an SDA targeting all the sensors from 25s to 40s (shown in the bottom part of the figure) without any protection. As can be seen in Figure 10a, without *DeLorean*, the rover's yaw angle estimates suffer heavy fluctuations (between -10 and +15 radian, should be constant without attack). As a result, the rover follows a bizarre path (a sketch is shown in Figure 10b), and does not reach its destination, thereby resulting in mission failure.

When *DeLorean* is deployed on the Aion rover, it prevents the yaw angle fluctuations due to the attack (Figure 10a). As a result, the rover navigates out of the attack zone. However, due to the attack, it missed the left turn it was supposed to execute (Figure 10b). Therefore, *DeLorean*'s course correction component successfully navigates the RV towards the target by calculating a new path. The small spikes in yaw angles with *DeLorean* in Figure 10a are due to the RV adjusting its position and heading direction to follow the new path (shown in curly blue lines in Figure 10b). Thus, *DeLorean* recovers the RV from the SDA and results in mission success.

TABLE V: *DeLorean* recovery under SDAs (single sensor and all sensors). Runtime, battery, and memory overheads

RV Type	Recovery success rate (%)		CPU Overhead	Battery Overhead	Memory Overhead
	Single	All Sensors			
Pixhawk	100	85	8.8%	22%	0.47 MB
Tarrot	100	90	6.7%	18.75%	0.45 MB
Sky-viper	100	80	9.2%	20%	0.52 MB
Aion R1	100	90	5.5%	14.4%	0.56 MB

#### D. Runtime, Memory and Battery Overheads of DeLorean

Table V shows the runtime and battery overheads incurred by *DeLorean* on the real RVs. The CPU overhead varies from

5.5% to 9.2%, with an average of 7.5% across the four RVs. This is slightly higher than the CPU overhead incurred by SSR and PID-Piper, which are 6.9% and 6.35% respectively (as reported in the respective papers).

*DeLorean*'s battery overhead is between 14.4% and 22% across RVs (18.87% on average). PID-Piper incurs about 1% battery overhead (SSR does not report battery overhead). While *DeLorean* incurs higher battery overhead than PID-Piper, it offers protection against multi-sensor SDAs unlike PID-Piper.

Finally, *DeLorean*'s memory overhead is between 0.45 MB to 0.56 MB across RVs. This memory overhead is less than 3% as many of our RVs have over 20 MB storage.

#### E. Need for Attack Diagnosis

To understand if attack diagnosis is needed, we compare *DeLorean*'s recovery with naive replay in recovering RVs. A naive replay technique replays historic states corresponding to all the sensors regardless of the number of sensors under attack (without diagnosis). In contrast, *DeLorean* performs attack diagnosis to identify the targeted sensors, and replays only the historic states corresponding to the targeted sensors.

TABLE VI: Mission success rate of Naive replay (without diagnosis) and *DeLorean*. No crashes occurred in both cases.

# of sensors targeted	Naive Replay	<i>DeLorean</i>
1	85.33%	100%
2	82.66%	100%
3	82.66%	100%
4	80.00 %	88%

In this experiment, we perform 75 missions each for *DeLorean* and naive replay techniques for the simulated RVs and attack 1-4 sensors in each mission (all combinations). Note that when all the 5 sensors are targeted, both *DeLorean* and naive replay would replay for all the sensors. Hence, we target up to 4 sensors. Table VI shows the average mission success rates for each category of missions. We find that both *DeLorean* and naive replay prevented crashes in all the cases. However, *DeLorean* had higher success rate than naive replay in all cases. naive replay only resulted in mission success rates between 80-85%. In contrast, *DeLorean* resulted in mission success rates between 88% and 100% in all cases. Further, *DeLorean* achieves 100% mission success when fewer than 4 sensors are targeted. Finally, even for failed missions, we find that the average deviation from the target incurred by *DeLorean* is 13.6m, whereas, the deviation incurred by naive replay is 20.2m on average. Thus, diagnosing the attack and selectively replaying historic states as done by *DeLorean* achieves higher a mission success than naive replay without any diagnosis.

#### F. Effectiveness of Attack Diagnosis

The previous section established the need for attack diagnosis. In this section, we investigate the effectiveness of the attack diagnosis by *DeLorean* by measuring its true positives (TP) and false positives (FP). TP is the fraction of times *DeLorean*'s diagnosis correctly identified the targeted sensors under an attack. FP is the fraction of times *DeLorean*'s diagnosis falsely identified sensors as attacked even in the absence of an attack.



We find that *DeLorean*'s diagnosis had 100% TPs. In all the mission shown in Table IV and Table V, *DeLorean*'s diagnosis correctly identified all the targeted sensors, and performed recovery by replaying the historic states corresponding to the targeted sensors. Further, *DeLorean* diagnosis did not identify any additional sensors that were not targeted by the attack.

To measure the FP rate of *DeLorean*'s diagnosis, the attack detector needs to (falsely) report an attack when there is none. Because we use a third-party attack detector, we cannot control when it reports false alarms. Therefore, we emulate a false alarm in the attack detector to study *DeLorean*'s diagnosis. Using the ArduCopter, we run 30 missions emulating a false alarm in the detector. We notice that in 90% of the cases, *DeLorean*'s diagnosis reports that no sensors were targeted by the attacker, and hence dismisses the detection as a false alarm. This is because the diagnosis mechanism independently analyses the error between the past and present states corresponding to the sensors in the RV, to identify attacks (Section IV-A).

In the remaining 10% of the cases, *DeLorean*'s diagnosis mechanism also falsely identified a sensor as being under attack, even when no attack was launched (10% FP rate). However, even in these cases, *DeLorean* performed a gratuitous recovery, and completed the mission successfully (100% mission success). We find that *DeLorean*'s gratuitous recovery resulted in 11.2% battery overhead. However, this overhead is incurred only in the rare event that *both the attack detector and DeLorean's attack diagnosis mechanisms report an FP*. For example, if the attack detector has a FP rate of 10% (based on the value reported in PID-Piper's paper [28]), and *DeLorean* has an FP rate of 10%, the probability of this event is 1%.

### G. Adaptive Attacks

We evaluate *DeLorean* under three adaptive attacks to test if an adversary who knows *DeLorean*'s recovery strategy can subvert it. The three attacks correspond to attackers who (1) launch SDAs at multiple geographical locations while preventing *DeLorean* from recording the most recent historic states for recovery. (2) choose a long attack duration such that *DeLorean* does not have sufficient recorded states to maneuver the RV out of the attack zone. (3) attempt to corrupt the historic states through stealthy attacks [27]), and thereby trick *DeLorean* into using the corrupted historic states for recovery.

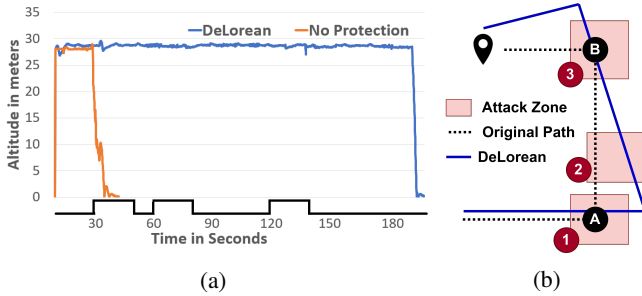


Fig. 11: *DeLorean*'s recovery in multi-zone SDA scenario. (a) with and without *DeLorean*, SDA launched 30-40s, 60-80s, 120-140s (bottom graph), (b) RV's trajectory under recovery.

**SDA in multiple zones:** For studying the impact of the first

attack on *DeLorean*, we perform an experiment on ArduCopter, and launch SDAs targeting all the sensors at 3 different zones during the mission. Figure 11b shows the original mission path where the RV attains an altitude of 30m, navigates towards A, takes a left turn and navigates towards B, and finally lands at the target. SDAs were launched at 1, 2, 3 for 20s.

Figure 11a shows *DeLorean*'s recovery. The first instance of SDA is launched at 30s. As can be seen, without *DeLorean* the drone crashes. In contrast, *DeLorean* replays the historic states recorded in 10-25.5s window (Table VII) and recovers the drone, as can be seen in Figure 11a altitude maintained at 30m. However, due to recovery activation, the drone missed the left turn. The course correction module detects the deviation, and calculates a new path to B. The second instance of SDA is launched at 60s. Recall that for ArduCopter the window size is 15.5s (Table VII), because *DeLorean* could not record a new set of historic states before the onset of the second SDA, it replays the historic states recorded in 10-15.5s window. As can be seen in Figure 11a, *DeLorean* maintains the drone's altitude at 30m between  $t=60$  to  $t=80$ s. Thus, *DeLorean* successfully recovers the drone from the second SDA. The third instance of SDA was launched at 120s. *DeLorean* replays the most recent historic states and recovers the drone from the third SDA as well (altitude maintained at 30m between 120-140 as shown in Figure 11a). Once the drone is out of the attack zone, the course correction module recalculates a path to the target, and the drone successfully completes the mission.

**Long Duration Attack:** We mount this attack on the Pixhawk drone. Recall that when the attack range is larger than distance covered by the recorded states, *DeLorean* iteratively replays the historic states until the RV is out of the attack zone. In this mission, *DeLorean* records the historic states in the window H1 ( $t=10$  to 15s). We launch both attacks (first single sensor SDA then multi-sensor SDA) for a duration that is 5X larger than the window H1. At  $t=15$ s, we launch a single sensor SDA targeting the gyroscope sensor. At  $t=20$ s, we launch an SDA targeting all the sensors.

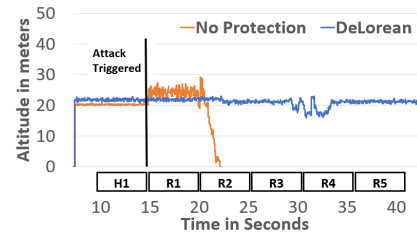


Fig. 12: *DeLorean*'s recovery for the Pixhawk drone when the attack duration is much larger than the recording window.

Figure 12 shows *DeLorean*'s recovery on the Pixhawk drone under the attacks. As can be seen, without *DeLorean*, in the window R2, the drone crashes due to the SDA. However, by iteratively replaying the historical states, *DeLorean* is able to prevent the crash, and maintain the altitude of the drone at 20m for the entire duration of the attack (from 15-40s). Thus, *DeLorean* is able to recover the RV from long duration attacks.

**Stealthy Attacks** We set a recording window large enough that a stealthy attack can be detected in one sliding window using CUSUM [28]. We assume that the attacker can perform both



a stealthy attack and an SDA simultaneously to deceive *DeLorean*. Instead of performing the stealthy attack persistently, she would perform stealthy attacks arbitrarily just to corrupt the recorded states. Then, the attacker would strategically perform an SDA which would trigger recovery activation. Because the arbitrarily performed stealthy attack remains undetected, *DeLorean* will replay the corrupted historic states.

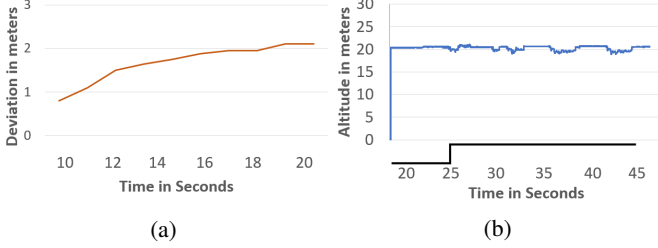


Fig. 13: *DeLorean*'s recovery in ArduCopter under stealthy attacks. (a) Corruptions in recorded states due to stealthy attacks, (b) Recovery under SDA targeting all the sensors.

We perform experiments on the ArduCopter to understand the impact of arbitrarily performed stealthy attacks on *DeLorean*. We assume that the attacker can perform stealthy attacks that either target a single sensor or all the sensors of the RV, while avoiding detection for as long as possible. We performed a stealthy attack arbitrarily from 10-20s while ensuring that the stealthy attack remains undetected. This caused a total deviation of 2.1m from the drone's original path (Figure 13a). *DeLorean* recorded the corrupted historic states as no alarm was raised by the attack detector. From 25-45s we launched an SDA, which is detected instantly, and *DeLorean* activates recovery (Figure 13b). As can be seen, *DeLorean* is able to recover the drone and maintain the altitude at 20m despite the corruptions in the recorded states due to the attack. This is because stealthy attacks have to be performed persistently to cause disruptions [27]. The corruption in historic states due to the arbitrarily performed stealthy attack is negligible, and hence replaying them does not disrupt the RV's mission.

## VII. LIMITATIONS AND DISCUSSION

**Obstacles on the RV's path** Our experiments do not include recovery in scenarios where there are obstacles in the mission path. Most industrial RVs today operate in open environments, e.g., a drone flies hundreds of meters above the ground [15]. However, in scenarios where obstacles are expected in the mission path, *DeLorean* will require supplementary recovery components to avoid the obstacles and safely maneuver the RV. Techniques have been proposed to leverage geometric characteristics of the RV's trajectory and derive commands to avoid obstacles [30]. In particular, they can find a direction for avoiding the obstacle and optimize the velocity vector. *DeLorean* can be equipped with obstacle avoidance systems to adjust the heading direction and velocity vectors under recovery to maneuver the RV safely around obstacles.

**Advanced Sensors** We evaluate *DeLorean* on GPS, gyroscope, accelerometer, magnetometer, and barometer sensors that can be manipulated through physical attacks that inject

fake signals. The autonomous operations in most industrial RVs today rely on the aforementioned sensors [13], [15]. Recently however, RV manufacturers have started using advanced sensors such as camera and LiDAR [14]. Attacks have been demonstrated targeting both the camera and LiDAR to deceive the machine learning models (ML) that are used for image classification [21], [37]. However, these attacks are out of our scope as they are crafted for specialized ML models.

## VIII. RELATED WORK

Physical attacks through GPS spoofing, optical sensor spoofing, acoustic signals and magnetic signals have been demonstrated against RVs [29], [41], [42], [46], autonomous vehicles [37], [45], and smart devices [41], [49]. Many attack detection techniques have been proposed for RVs [18], [25], [28], [38], [43], [50], and other cyber physical systems (CPS) [16], [23], [32] that detect attacks based on either invariants or model estimations. However, these techniques focus only on attack detection, and provide neither attack diagnosis nor recovery, which are important for RVs.

To our knowledge, only two techniques, SSR and PID-Piper have demonstrated attack recovery in real RVs [24], [28]. We have studied these in detail earlier. Reinforcement learning (RL) has been proposed for recovering RVs from faults and attacks [31]. However, this technique requires the policy to be trained with representative faults and attacks, to distinguish them from normal operation, which are difficult to obtain in practice. Further, unlike *DeLorean*, this technique requires manual remediation to handle certain types of attacks.

A recent paper uses reachability analysis to recover CPS from attacks [51]. There are three main differences with our work. First, they do not perform attack diagnosis. Rather, the technique considers all sensors as being under attack in every case, which as we have seen earlier, is much less effective than targeted diagnosis and recovery. Second, they consider a simple attack scenario where the attack is confined to a 5-6s window, and the attacker injects only small bias values into the sensors. In contrast, we consider strong attacks, as well as adaptive attacks such as long duration attacks and stealthy attacks. Finally, they consider a recovery to be successful if the CPS reaches a reference point within a safety deadline, regardless of whether the RV completes the mission. On the other hand, *DeLorean* considers a recovery to be successful if and only if the RV completes its mission without crashing.

## IX. CONCLUSION

We presented *DeLorean*, an attack diagnosis and attack recovery framework for securing RVs from Sensor Deception Attacks (SDAs). SDAs are physical attacks that can manipulate the values of one or more of the RV's sensors (including those of multiple types). *DeLorean* inspects the attack induced errors in the RV's physical states using factor graphs, and identifies the targeted sensors by SDA. It then isolates the targeted sensors from the RV's feedback control loop, and replays a sequence of historic states recorded from an attack-free phase of the RV mission to derive safe actuator signals, thereby maneuvering the RV out of the attack zone.

We evaluate *DeLorean* on 4 real RVs and 2 simulated RVs. We find that *DeLorean* (1) recovers RVs from all SDAs without

crashing, and achieves mission success in about 94% of the cases on average (82% in the worst case when all sensors are targeted), (2) prevents crashes and ensures mission success against adaptive attacks, and (3) incurs performance (7.5% on average) and memory overheads (3% on average), and battery overheads of about 19% on average.

## REFERENCES

- [1] "Agris t16 - agriculture spraying drone," <https://www.dji.com/ca/t16>.
- [2] "Aion r1 ardupilot edition," <https://docs.aionrobotics.com/en/latest/r1-ugv.html>.
- [3] "Amazon robotics," <https://robots.ieee.org/robots/kiva/>.
- [4] "Ardupilot - software in the loop," <http://ardupilot.org/dev/docs/sitl-simulator-software-in-the-loop.html>.
- [5] "Gazebo robot simulation," <http://gazebo-sim.org/>.
- [6] "Noise sources and their effects," <https://www.chem.purdue.edu/chemsafety/Training/PPETrain/dblevels.htm>.
- [7] "Official u.s. government information about the global positioning system (gps) and related topics," <https://www.gps.gov/technical/ps/2008-SPS-performance-standard.pdf>.
- [8] "Pid-piper code," <https://github.com/DependableSystemsLab/pid-piper>.
- [9] "Sky viper journey drone," <https://sky-viper.com/journey/>.
- [10] "System identification overview," <https://www.mathworks.com/help/ident/gs/about-system-identification.html>.
- [11] "Tarot 650 v2 drone," <https://uavsystemsinternational.com/products/tarot-650-ready-to-fly-drone>.
- [12] "u-blox m8 concurrent gnss modules," <https://www.u-blox.com/en/product/neo-m8-series>.
- [13] "Walmart drone delivery," <https://www.droneup.com/>.
- [14] "Wingcopter," <https://wingcopter.com/wingcopter-198>.
- [15] "Zipline drone delivery," <http://www.flyzipline.com/>.
- [16] C. M. Ahmed, J. Zhou, and A. P. Mathur, "Noise matters: Using sensor and process noise fingerprint to detect stealthy cyber attacks and authenticate sensors in cps," in *Proceedings of the 34th Annual Computer Security Applications Conference*, ser. ACSAC '18. New York, NY, USA: ACM, 2018, pp. 566–581. [Online]. Available: <http://doi.acm.org/10.1145/3274694.3274748>
- [17] D. M. Bevilacqua and B. Parkinson, "Cascaded kalman filters for accurate estimation of multiple biases, dead-reckoning navigation, and full state feedback control of ground vehicles," *IEEE Transactions on Control Systems Technology*, vol. 15, no. 2, pp. 199–208, 2007.
- [18] A. Bezemskij, G. Loukas, R. J. Anthony, and D. Gan, "Behaviour-based anomaly detection of cyber-physical attacks on a robotic vehicle," in *2016 15th International Conference on Ubiquitous Computing and Communications and 2016 International Symposium on Cyberspace and Security (IUCC-CSS)*, Dec 2016, pp. 61–68.
- [19] P. Cao, E. Badger, Z. Kalbarczyk, R. Iyer, and A. Slagell, "Preemptive intrusion detection: Theoretical framework and real-world measurements," in *Proceedings of the 2015 Symposium and Bootcamp on the Science of Security*, ser. HotSoS '15. New York, NY, USA: Association for Computing Machinery, 2015. [Online]. Available: <https://doi.org/10.1145/2746194.2746199>
- [20] Y. Cao, N. Wang, C. Xiao, D. Yang, J. Fang, R. Yang, Q. A. Chen, M. Liu, and B. Li, "Invisible for both camera and lidar: Security of multi-sensor fusion based perception in autonomous driving under physical-world attacks," *2021 IEEE Symposium on Security and Privacy (SP)*, May 2021. [Online]. Available: <http://dx.doi.org/10.1109/SP40001.2021.00076>
- [21] Y. Cao, C. Xiao, D. Yang, J. Fang, R. Yang, M. Liu, and B. Li, "Adversarial objects against lidar-based autonomous driving systems," *arXiv preprint arXiv:1907.05418*, 2019.
- [22] W. Chen, Y. Dong, and Z. Duan, "Attacking altitude estimation in drone navigation," in *IEEE INFOCOM 2018 - IEEE Conference on Computer Communications Workshops (INFOCOM WKSHPS)*, 2018, pp. 888–893.
- [23] Y. Chen, C. M. Poskitt, and J. Sun, "Learning from mutants: Using code mutation to learn and monitor invariants of a cyber-physical system," in *2018 IEEE Symposium on Security and Privacy (SP)*. Los Alamitos, CA, USA: IEEE Computer Society, may 2018, pp. 648–660. [Online]. Available: <https://doi.ieeecomputersociety.org/10.1109/SP.2018.00016>
- [24] H. Choi, S. Kate, Y. Aafer, X. Zhang, and D. Xu, "Software-based realtime recovery from sensor attacks on robotic vehicles," in *23rd International Symposium on Research in Attacks, Intrusions and Defenses (RAID 2020)*. San Sebastian: USENIX Association, Oct. 2020, pp. 349–364.
- [25] H. Choi, W.-C. Lee, Y. Aafer, F. Fei, Z. Tu, X. Zhang, D. Xu, and X. Deng, "Detecting attacks against robotic vehicles: A control invariant approach," in *Proceedings of the 2018 ACM SIGSAC Conference on Computer and Communications Security*, ser. CCS '18. New York, NY, USA: ACM, 2018, pp. 801–816. [Online]. Available: <http://doi.acm.org/10.1145/3243734.3243752>
- [26] A. A. Clements, N. Almakhdhub, K. S. Saab, P. Srivastava, J. Koo, S. Bagchi, and M. Payer, "Protecting bare-metal embedded systems with privilege overlays," in *2017 IEEE Symposium on Security and Privacy (SP)*. Los Alamitos, CA, USA: IEEE Computer Society, may 2017, pp. 289–303. [Online]. Available: <https://doi.ieeecomputersociety.org/10.1109/SP.2017.37>
- [27] P. Dash, M. Karimibiuki, and K. Pattabiraman, "Out of control: Stealthy attacks against robotic vehicles protected by control-based techniques," in *Proceedings of the 35th Annual Computer Security Applications Conference*, ser. ACSAC '19. New York, NY, USA: ACM, 2019, pp. 660–672. [Online]. Available: <http://doi.acm.org/10.1145/3359789.3359847>
- [28] P. Dash, G. Li, Z. Chen, M. Karimibiuki, and K. Pattabiraman, "Pid-piper: Recovering robotic vehicles from physical attacks," in *2021 51st Annual IEEE/IFIP International Conference on Dependable Systems and Networks (DSN)*, 2021, pp. 26–38.
- [29] D. Davidson, H. Wu, R. Jellinek, V. Singh, and T. Ristenpart, "Controlling uavs with sensor input spoofing attacks," in *10th USENIX Workshop on Offensive Technologies (WOOT 16)*. Austin, TX: USENIX Association, Aug. 2016. [Online]. Available: <https://www.usenix.org/conference/woot16/workshop-program/presentation/davidson>
- [30] J. Dentler, S. Kannan, M. A. O. Mendez, and H. Voos, "A real-time model predictive position control with collision avoidance for commercial low-cost quadrotors," in *2016 IEEE Conference on Control Applications (CCA)*, 2016, pp. 519–525.
- [31] F. Fei, Z. Tu, D. Xu, and X. Deng, "Learn-to-recover: Retrofitting uavs with reinforcement learning-assisted flight control under cyber-physical attacks," in *2020 IEEE International Conference on Robotics and Automation (ICRA)*, 2020, pp. 7358–7364.
- [32] M. Gauthama Raman, W. Dong, and A. Mathur, "Deep autoencoders as anomaly detectors: Method and case study in a distributed water treatment plant," *Computers and Security*, vol. 99, p. 102055, 2020. [Online]. Available: <https://www.sciencedirect.com/science/article/pii/S016740482030328X>
- [33] D. Hambling, "Uk ship hit by gps spoof," *New Scientist*, vol. 250, no. 3341, p. 17, 2021. [Online]. Available: <https://www.sciencedirect.com/science/article/pii/S0262407921011313>
- [34] K. Hartmann and C. Steup, "The vulnerability of uavs to cyber attacks-an approach to the risk assessment," in *13th international conference on cyber conflict (CYCON 2013)*. IEEE, 2013, pp. 1–23.
- [35] A. J. Hawkins, "Ups will use drones to deliver medical supplies in north carolina." [Online]. Available: <https://www.theverge.com/2019/3/26/18282291/ups-drone-delivery-hospital-nc-matternet>
- [36] T. E. Humphreys, "Assessing the spoofing threat: Development of a portable gps civilian spoofer," in *In Proceedings of the Institute of Navigation GNSS (ION GNSS)*, 2008.
- [37] X. Ji, Y. Cheng, Y. Zhang, K. Wang, C. Yan, W. Xu, and K. Fu, "Poltergeist: Acoustic adversarial machine learning against cameras and computer vision," in *2021 IEEE Symposium on Security and Privacy (SP)*. IEEE, 2021, pp. 160–175.
- [38] A. Khan, H. Kim, B. Lee, D. Xu, A. Bianchi, and D. J. Tian, "M2mon: Building an mmio-based security reference monitor for unmanned vehicles," in *30th {USENIX} Security Symposium ({USENIX} Security 21)*, 2021.

- [39] L. Ljung, "Asymptotic behavior of the extended kalman filter as a parameter estimator for linear systems," *IEEE Transactions on Automatic Control*, vol. 24, no. 1, pp. 36–50, February 1979.
- [40] L. Meier, P. Tanskanen, F. Fraundorfer, and M. Pollefeys, "Pixhawk: A system for autonomous flight using onboard computer vision," in *2011 IEEE International Conference on Robotics and Automation*. IEEE, 2011, pp. 2992–2997.
- [41] S. Nashimoto, D. Suzuki, T. Sugawara, and K. Sakiyama, "Sensor con-fusion: Defeating kalman filter in signal injection attack," in *Proceedings of the 2018 on Asia Conference on Computer and Communications Security*, ser. ASIACCS '18. New York, NY, USA: Association for Computing Machinery, 2018, p. 511–524. [Online]. Available: <https://doi.org/10.1145/3196494.3196506>
- [42] J. Noh, Y. Kwon, Y. Son, H. Shin, D. Kim, J. Choi, and Y. Kim, "Tractor beam: Safe-hijacking of consumer drones with adaptive gps spoofing," *ACM Transactions on Privacy and Security (TOPS)*, vol. 22, no. 2, pp. 1–26, 2019.
- [43] R. Quinonez, J. Giraldo, L. Salazar, E. Bauman, A. Cardenas, and Z. Lin, "SAVIOR: Securing autonomous vehicles with robust physical invariants," in *29th USENIX Security Symposium (USENIX Security 20)*. Boston, MA: USENIX Association, Aug. 2020.
- [44] C. Reimann, P. Filzmoser, and R. G. Garrett, "Background and threshold: critical comparison of methods of determination," *Science of The Total Environment*, vol. 346, no. 1, pp. 1–16, 2005. [Online]. Available: <https://www.sciencedirect.com/science/article/pii/S0048969704007983>
- [45] Y. Shoukry, P. Martin, P. Tabuada, and M. Srivastava, "Non-invasive spoofing attacks for anti-lock braking systems," in *Cryptographic Hardware and Embedded Systems - CHES 2013*, G. Bertoni and J.-S. Coron, Eds. Berlin, Heidelberg: Springer Berlin Heidelberg, 2013, pp. 55–72.
- [46] Y. Son, H. Shin, D. Kim, Y. Park, J. Noh, K. Choi, J. Choi, and Y. Kim, "Rocking drones with intentional sound noise on gyroscopic sensors," in *24th USENIX Security Symposium (USENIX Security 15)*. Washington, D.C.: USENIX Association, 2015, pp. 881–896. [Online]. Available: <https://www.usenix.org/conference/usenixsecurity15/technical-sessions/presentation/son>
- [47] N. O. Tippenhauer, C. Pöpper, K. B. Rasmussen, and S. Capkun, "On the requirements for successful gps spoofing attacks," in *Proceedings of the 18th ACM Conference on Computer and Communications Security*, ser. CCS '11. New York, NY, USA: ACM, 2011, pp. 75–86. [Online]. Available: <http://doi.acm.org/10.1145/2046707.2046719>
- [48] T. Trippel, O. Weisse, W. Xu, P. Honeyman, and K. Fu, "Walnut: Waging doubt on the integrity of mems accelerometers with acoustic injection attacks," in *2017 IEEE European Symposium on Security and Privacy (EuroS P)*, April 2017, pp. 3–18.
- [49] Y. Tu, Z. Lin, I. Lee, and X. Hei, "Injected and delivered: Fabricating implicit control over actuation systems by spoofing inertial sensors," in *27th USENIX Security Symposium (USENIX Security 18)*. Baltimore, MD: USENIX Association, Aug. 2018, pp. 1545–1562. [Online]. Available: <https://www.usenix.org/conference/usenixsecurity18/presentation/tu>
- [50] N. Xue, L. Niu, X. Hong, Z. Li, L. Hoffaeller, and C. Pöpper, "Deepsim: Gps spoofing detection on uavs using satellite imagery matching," in *Annual Computer Security Applications Conference*, ser. ACSAC '20. New York, NY, USA: Association for Computing Machinery, 2020, p. 304–319. [Online]. Available: <https://doi.org/10.1145/3427228.3427254>
- [51] L. Zhang, P. Lu, F. Kong, X. Chen, O. Sokolsky, and I. Lee, "Real-time attack-recovery for cyber-physical systems using linear-quadratic regulator," *ACM Trans. Embed. Comput. Syst.*, vol. 20, no. 5s, sep 2021. [Online]. Available: <https://doi.org/10.1145/3477010>

## APPENDIX

### A. Joint Probability and Factor Graphs

The joint probability of variables  $x_1, \dots, x_n$  is described as  $P(x_1, \dots, x_n)$ . Causal inference of an event given the observed variable is calculated as:  $y = \operatorname{argmax}_y P(y|x_1, \dots, x_{n-1})$ , which

can be further expanded as the following.

$$P(y|x_1, \dots, x_{n-1}) = \frac{P(x_1, \dots, x_{n-1})}{\sum_v P(x_1, \dots, x_{n-1}, y = v)} \quad (5)$$

Inference on a joint probability distribution  $P(x_1, \dots, x_n)$  requires  $2^n$  storage for events with binary outcome (e.g., malicious, benign), which is computationally expensive as well.

Factor graphs can be used to overcome this problem. A factor graph (FG) is probabilistic graphical model that allows expressing joint probability as product of smaller local functions [19]. Figure 14 shows an example. There are two types of nodes in a FG namely variables ( $x_1, x_2, x_3$ ) and factor functions ( $f_1, f_2, f_3$ ). Variables are used to quantitatively describe an event. A factor function is used to express relationship among variables.

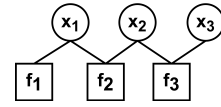


Fig. 14: An example of factor graph

Let's take Figure 14 as an example to understand how to calculate conditional probability using factor graph. The variables  $x_1, x_2, x_3 \in X$ , and  $y$  is the outcome.  $P(x_1, x_2, x_3)$  can be factored as a product of  $f_1, f_2, f_3$ .

$$P(x_1, x_2, x_3) = f_1(x_1) \cdot f_2(x_1, x_2) \cdot f_3(x_2, x_3) \quad (6)$$

Thus, conditional probability of an event given the observed variables is calculated as:

$$P(y|x_1, x_2, x_3) = \prod_{f \in F} f(x) \quad (7)$$

Using sum product algorithm, the marginal is defined as  $P(x) = \sum_{x \in X} P(X)$ . Thus, the conditional probability of an event given the observed variables is calculated as the following.

$$P(y|x_1, x_2, x_3) = \sum f(x) \quad (8)$$

### B. Erroneous Physical States due to SDA

Figure 15 shows the attack induced error in RV's physical states for the experiment discussed in Section III. In this experiment, we intermittently launched 4 instances of SDA at  $t=10s$ ,  $t=20s$ ,  $t=35s$ , and  $t=45s$ , targeting all the onboard sensors. The first 3 instances of SDA lasted for 1s. In contrast, the fourth instance of SDA lasted for more than 5s, which caused the RV to crash.

For simplicity, we show 2 out of 15 physical states of the RV. Figure 15a and Figure 15b shows the change of roll angle and pitch angles respectively under SDA. Note that as the drone is navigating in a straight line at a fixed altitude, the roll angle should be 0, because the drone is not rotating along its  $x$  axis. Similarly, after takeoff, the drone's pitch angle should be constant as the drone is not gaining elevation. As we can see in Figure 15a, during the attack free phase of the mission (0-10s), the roll angle is 0 degrees. The attack starts after 10s, and as a result, the roll rate fluctuates between  $-30$  and  $+30$  degrees (Figure 15a). Similar trends can be seen for pitch angle

TABLE VII:  $\delta$  values for per sensor factor graphs in each subject RVs. position  $(x, y, z)$  in meters (m), velocity  $(\dot{x}, \dot{y}, \dot{z})$  in  $m/s$ , acceleration  $(\ddot{x}, \ddot{y}, \ddot{z})$  in  $m/s^2$ , Euler angles  $(\phi, \theta, \psi)$  in degrees, angular velocities  $(\omega_\phi, \omega_\theta, \omega_\psi)$  in rad/s, magnetic fields  $(x_m, y_m, z_m)$  in Gauss(G), Altitude in m. (values are rounded up to 1st decimal place)

RV Type	GPS						Accel			Gyroscope						Mag			Baro	Window Size
	$x$	$y$	$z$	$\dot{x}$	$\dot{y}$	$\dot{z}$	$\ddot{x}$	$\ddot{y}$	$\ddot{z}$	$\phi$	$\theta$	$\psi$	$\dot{\phi}$	$\dot{\theta}$	$\dot{\psi}$	$x_m$	$y_m$	$z_m$	Alt	
Pixhawk	3.4	5.1	5.2	2.1	10.2	5.5	6.5	4.2	10.5	12.2	9.8	45.5	11.5	13.8	1.1	0.6	0.3	0.5	0.2	15.5s
Tarrot	5.5	3.4	6.5	1.8	8.1	4.2	8.1	7.7	9.2	10.2	9.5	38.9	10.2	10.6	1.1	0.3	0.3	0.4	0.2	15s
Sky-Viper	4.6	3.0	4.1	1.7	7.8	3.1	5.5	4.2	5.6	13.3	11.2	58.5	14.5	16.1	1.5	0.6	0.6	0.5	0.2	17s
AionR1	2.7	2.5	-	1.9	6.4	-	3.3	3.5	-	-	-	45.2	-	-	2.2	-	-	-	-	18.5s
ArduCopter	3.7	3.3	4.5	2.1	9.3	4.2	5.2	6.5	7.1	9.7	9.5	36.2	9.5	11.2	1.1	0.3	0.2	0.5	0.1	15.5s
ArduRover	4.2	4.1	-	2.4	7.3	-	3.5	3.9	-	-	-	38.5	-	-	1.8	-	-	-	-	17s

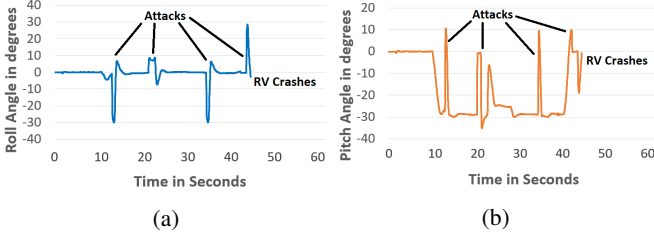


Fig. 15: (a) Roll angle fluctuations, (b) Pitch angle fluctuations of Pixhawk drone due to SDA targeting all the sensors simultaneously.

(Figure 15b), just before the attack started the pitch angle was set at -30 degrees and should remain constant for the entire duration of the mission. Under attack, the pitch angle fluctuates between -35 and +12 degrees. Thus, attack induced sensor manipulations result in erroneous physical states.

### C. Course Correction

Algorithm 2 shows the steps for course correction. Once the attack subsides based on attack detector's response, *DeLorean* checks if the RV has veered off its trajectory (Line 10). If so, *DeLorean* activates course correction and calculates a new path to the next waypoint (Line 11-12). The RV's navigation module is updated as per the new path (Line 13). To avoid the RV from going back into the attack zone, the weight of the path being recovered from is increased (Line 14). To handle case where the RV's destination is in the attack zone, we add a check in the course correction algorithm to check if the total distance traveled without recovery ( $d_t$ ) and with recovery ( $d_a$ ) is  $\geq$  distance to destination (Line 18-19), if so, we signal to complete the mission.

### D. Mission Types and Per-Sensor Factor Graph

Table VII shows the  $\delta$  values for attack diagnosis for all the subject RV. Table VIII shows the mission details.

Mission Paths	S	MW	C	P1	P2	P3
Number of missions	15	15	15	10	10	10

TABLE VIII: Mission paths used in Evaluating *DeLorean*. S: Straight line, MW: Multiple waypoints, P1:Polygonal-1, P2:Polygonal2, P3:Polygonal-3

### Algorithm 2 Algorithm for Course Correction

```

1:  $D \leftarrow$  distance to destination
2:  $d_t \leftarrow$  distance traveled
3:  $d_g \leftarrow$  distance to cover
4:  $d_a \leftarrow$  distance traveled under attack
5:  $p_i \leftarrow$  original mission path
6:  $p_a \leftarrow$  path under recovery
7:  $p_r \leftarrow$  path during course correction
8: procedure COURSE CORRECTION
9:   if !alert and recovery_mode  $\leftarrow$  true then
10:    if  $D > d_t + d_g + d_a$  then
11:      source  $\leftarrow$  GPS() ▷ current Location
12:       $p_r \leftarrow$  shortest_path(source, destination)
13:      update_nav( $p_r$ ) ▷ update mission trajectory
14:       $p_a \leftarrow w * x$  ▷ update weight of  $p_a$ 
15:    end if
16:  else
17:     $d_a \leftarrow$  update  $d_a$ 
18:    if  $D > d_t + d_a$  then
19:      command  $\leftarrow$  complete mission
20:    end if
21:  end if
22: end procedure

```

### E. Physical States Error under Recovery

Figure 16a shows the error in the target and the current physical state ( $e_s = \text{target} - \text{current}$ ) of the Pixhawk drone under recovery. An SDA targeting all the sensors was launched from  $t=25$  to  $45s$ . Without *DeLorean* the error  $e_s$  fluctuates due to the SDA (Section III). In contrast, with *DeLorean* the error in RV's physical states remains bounded. As can be seen in Figure 16a, under recovery, the error in RV's roll and pitch angles remain bounded between -0.25 and +0.25 degrees. As the corruptions in the PID controller's input are controlled, the PID controller derives constant actuator signals which safely maneuvers the RV. Figure 16b shows the output of motor-1 as an example which is set at 0.65 under recovery.

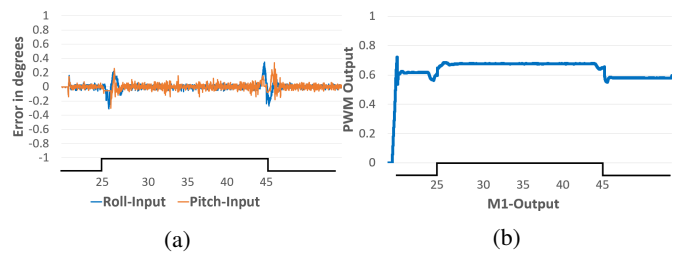


Fig. 16: (a) Roll and Pitch angle under recovery (b) Actuator signal under recovery of Pixhawk drone